Channel Measurements and Modeling for a 60 GHz Wireless Link Within a Metal Cabinet

Seyran Khademi, *Student Member, IEEE*, Sundeep Prabhakar Chepuri, *Student Member, IEEE*, Zoubir Irahhauten, *Member, IEEE*, Gerard J. M. Janssen, *Member, IEEE*, and Alle-Jan van der Veen, *Fellow, IEEE*

***Abstract*—This paper presents the channel measurements performed within a closed metal cabinet at 60 GHz covering the frequency range 57–62 GHz. Two different volumes of an empty metal cupboard are considered to emulate the environment of interest (an industrial machine). Furthermore, we have considered a number of scenarios such as line of sight, non line of sight, and placing absorbers. A statistical channel model is provided to aid short-range wireless link design within such a reflective and confined environment. Based on the measurements, the large- and small-scale parameters are extracted and fitted using the standard log-normal and Saleh–Valenzuela models, respectively. The obtained results are characterized by a very small path loss exponent, a single cluster phenomenon, and a significantly large root-mean-square (RMS) delay spread. The results show that covering a wall with absorber material dramatically reduces the RMS delay spread. Finally, the proposed channel model is validated by comparing the measured channel with a simulated channel, where the simulated channel is generated from the extracted parameters.**

***Index Terms*—Channel characterization and modeling, frequency-domain sounding, 60-GHz measurements, path loss, root-mean-square (RMS) delay spread.**

I. Introduction

A. Problem Context

INSIDE mechatronic and industrial machinery, the required wiring is an increasing concern, as it comes with issues like reliability, space efficiency, and flexibility. It thus becomes interesting to replace the wires by wireless connections. Literature refers to a so-called "wireless harness" for the communication between components inside machinery devices where the propagation distances are in the order of a few meters or less [2]. On the one hand, using multiple cables inside a dense area to connect moving parts within a confined space can significantly complicate the design and maintenance of the system. A wired connection to a moving part affects the dynamics and may cause cable jams and frequent damage to such machineries. On the other hand, current wireless technology does not meet the data rates offered by wired standards like gigabit Ethernet. To move towards a reliable and fast wireless connection for industrial use, many efforts have been made to provide suitable channel models for the wireless harness applications. In very small-scale applications such as inter chip connections [3] or board-to-board communications [4], [5], a noticeable difference, in terms of channel properties, has been reported in the literature compared with the typical indoor and UWB channels [6]–[10]. Also, Ohira *et al.* studied the propagation characteristic inside the information communication technology (ICT) equipments such as a printer, vending and automated teller machine (ATM) [11] which is the most relevant work in spirit to this paper as the channel is measured inside a metal enclosure (ME). Also, a simple communication system is tested for ICT devices and associated results are reported in [12].

The unlicensed multi-GHz spectrum available around 60 GHz has gained a lot of interest in the past decade for both indoor and outdoor applications [13]–[15]. Specifically, this millimeter-wave band has the ability to support short-range high data rates in the order of Gbps. Both 802.11ad and 802.15c are evolving standards based on this alternative bandwidth (BW) [16], [17]. As a result, many measurements have been conducted to model the propagation environment at 60 GHz. While the literature is mostly concentrated on indoor channel characterization at this band [18]–[21], channel models for outdoor implementation of wireless systems based on millimeter-wave have also been investigated [22]. However, there are numerous issues in long-distance communications in this band due to the large attenuation of radio waves because of oxygen absorption. A good survey on channel measurements in 60 GHz can be found in [23].

Channel characterization results for short-range wireless links in the 60 GHz band, have been reported in [17], [24], [25], however, the channel characterization for the so-called wireless harness applications[1] is not yet reported. The physically available bandwidth (BW) (at least 5 GHz) and small antenna size makes the 60 GHz band very appealing for wireless harness applications. Furthermore, the integration of antennas on small chips [26] can facilitate the deployment of the recently

Manuscript received September 10, 2014; revised January 16, 2015 and March 13, 2015; accepted April 28, 2015. Date of publication May 13, 2015; date of current version September 7, 2015. A portion of this work was presented at IEEE EuCAP, The Hague, the Netherlands, April 2014. This work was supported in part by STW under the FASTCOM Project (10551). The associate editor coordinating the review of this paper and approving it for publication was A. Zajic.

S. Khademi, S. P. Chepuri, G. J. M. Janssen, and A.-J. van der Veen are with the Faculty of Electrical Engineering, Mathematics and Computer Science, Delft University of Technology, 2628CD Delft, The Netherlands (e-mail: s.khademi@tudelft.nl; s.p.chepuri@tudelft.nl; g.j.m.janssen@tudelft.nl; a.j.vanderveen@tudelft.nl).

Z. Irahhauten is with the Mobile Innovation Radio Group, KPN, Den Haag 2500, The Netherlands (e-mail: zoubir.irahhauten@kpn.com).

Color versions of one or more of the figures in this paper are available online at http://ieeexplore.ieee.org.

Digital Object Identifier 10.1109/TWC.2015.2432755

[1] Kawasaki et al. studied the millimeter propagation environment for internal I/O connections in [3].

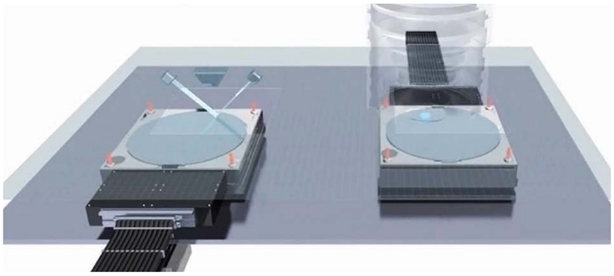

Fig. 1. An illustration of two moving wafer stages with their cables in a lithography system. The considered measurement scenarios emulate such lithography machines.

introduced large-MIMO systems [27] which could be a milestone in boosting the data rate in wireless systems.

The main contribution of this paper is to provide a statistical channel model for applications in 60 GHz band that operates inside a metal enclosure (ME).

B. Applications and Motivations

Lithography systems play a critical role in the development and manufacture of integrated circuits (ICs). The lithography process requires extremely accurate mask and substrate positioning. This task is performed via several sensors and actuators, which are typically connected to the control units via flat-cable wires. In this paper, we investigate the propagation environment for millimeter-waves inside a lithography system for developing a very high data rate (peak data rate up to a few tens of Gbps) wireless link between the positioning sensors and the control unit. This is fundamental for replacing the wired connections with wireless links.

The sensors and actuators are mounted on moving platforms that experience very high accelerations. The stiffness of the cables causes undesired disturbances to the system which leads to inaccurate positioning. Also, the trend towards increasing numbers of moving sensors makes the design of the wiring system prohibitively complex, therefore the replacement of the cables is of interest.

As we had limited access to an actual lithography machine, the measurements have been conducted inside a metal cabinet that was empty except for some cables, antennas and stand holders. The reproducible setup emulates the propagation environment in a wafer stage section within the lithography machine. This can be described as a metal drawer which is placed in the lithography device and includes two moving wafer stages as illustrated in Fig. 1.

This environment contains rather large amounts of open space, in contrast to the compact scenarios found in ICT devices, as investigated in the literature [11] . The initial experiments for establishing the wireless link within the ME show an extremely fading environment due to the reflections from the walls, which limits the data rate. Thus, the lack of proper channel models for such hallow and confined environments motivates the considered measurement campaign and modeling.

However, apart from the lithography machines, there are other systems that can benefit from this work, e.g., scenarios with wireless connections for possible sensors or devices inside an empty elevator or telecabine shaft. The empty cupboard can be viewed as an extreme case of a general ME. With absorbing objects inside the confined space, one can expect fewer reflections and shorter channel impulse responses (CIR).

C. Outline

In the context of this paper, we have made extensive measurements of channel frequency responses (CFRs) using a channel frequency domain (FD) sounding technique within the 57–62 GHz band. This has been done by placing the receiver on a pre-designed spatial grid, step by step, while the transmitter is fixed. The power delay profile (PDP) and multipath components (MPCs) are extracted by post processing. Two different volumes of the metal cupboard are used and the measurements are provided for both the LOS and NLOS scenarios. The results indicate that the environments within MEs are highly reflective, and the resulting "long" wireless channels will make wireless communications very challenging. Also, the fading properties change depending on the volume of the cupboard rather than the LOS and NLOS situations. We have also used absorbers to cover a metal wall for one scenario which resulted in a significant reduction in the root-mean-square (RMS) delay spread (RDS) and this consequently affects the fading properties of the channel.

Both small-scale and large-scale channel model parameters are extracted from the measurements, based on the well-known Saleh-Valenzuela (SV) [28] and log-normal model [29], [30], respectively. Accordingly, a comprehensive statistical channel model is provided to simulate similar fading channels. Random channel instances are generated based on the extracted parameters for arrival time, time decay constant, and number of paths. Next, the RDS properties of the simulated and measured channels are compared. The purpose of this verification is twofold. Firstly, it assures whether the number of measurements is sufficient for extracting the parametric statistical channel model. Secondly, it validates the accuracy of the model itself. Together with the Doppler frequency change (time variance property), the proper channel instances can be simulated via the Matlab channel modeling toolbox [31] or other off-the-shelf simulation software based on SV or stochastic tap-delay-line (STDL) models [7], [32].

The remainder of this paper is organized as follows. In Section II-A, we describe the measurement set-up and explain the measurement procedure. In Section II-B, we provide details regarding data processing to extract parameters required for channel modeling. Based on these parameters, large-scale (path loss) and small-scale channel models (RDS) are presented in Sections III and IV, respectively. The proposed statistical channel parameters based on the SV model (time decay constant and arrival rates) are given in Section V. The proposed channel model is validated together with the coherence time and bandwidth of the system in Section VI. Also, we compare the statistical parameters for the measured channels with the SV channel model suggested for the IEEE 802.15 standard and other related measurements in the literature. Final remarks are made in Section VII.

II. Measurement Set-up and Procedure

In this section, the channel measurement procedure and details of the equipments used for the measurements are explained.

Channel characterization can be performed in either time domain (TD) or FD [33]. In the measurements provided in this paper, a FD sounding technique is used. The scattering parameters (i.e., S_{11}, S_{12}, S_{21}, and S_{22}) are measured using a vector network analyzer (VNA) by transmitting sinusoidal waves at discrete frequencies. The frequency spacing, Δf_s, and the scanned BW, B_w, determines the maximum measurable excess delay, τ_{max}, and the resolution of the captured multipaths, τ_{res}, respectively, and they are given as

$$\Delta f_s = \frac{B_w}{N_s - 1}, \quad \tau_{max} = \frac{1}{\Delta f_s}, \quad \tau_{res} = \frac{1}{B_w}, \tag{1}$$

where N_s is the number of transmitted sinusoidal waves.

The frequency domain S_{21} parameter is generally referred to as CFR. The CIR is obtained from the measured CFR by taking the inverse fast Fourier transform (IFFT). A Hann window is applied to reduce the effect of side lobes.

A. Measurement Set-Up

The measurement BW is set to $B_w = 5$ GHz, and the channel is sampled from 57 GHz to 62 GHz at $N_s = 12001$ frequency points. This results in a frequency spacing of $\Delta f_s = 0.416$ MHz, so that the time resolution is $\tau_{res} = \frac{1}{B_w} = 0.2$ ns and the maximum measurable excess delay is $\tau_{max} = 2400$ ns. The CFR is measured using a PNA-E series microwave VNA E8361A from Agilent. An intermediate frequency BW of $B_{IF} = 50$ Hz is chosen to reduce the noise power within the measurement band, which improves the dynamic range. This is the receiver BW for single sinusoid in a VNA; the smaller intermediate frequency BW leads to a larger signal to noise ratio. Also each measurement is repeated 50 times to further average out the noise.

Due to the losses inside the VNA and 60 GHz co-axial cables, the measured signal at the receiver is weak. A 60 GHz solid state power amplifier (PA) from QuinStar Inc. (QGW-50662030-P1) is used to compensate for the losses and to further improve the dynamic range. An illustration of the measurement set-up is provided in Fig. 2. For the transmit and receive antennas, we have used two identical open waveguide antennas operating in 50-75 GHz frequency band with aperture size 3.759×1.880 mm^2. The beam pattern of the antennas is shown in Fig. 3. The gain of the open waveguide antenna is about 4.6 dBi (see [34] for details on computing the gain).

The near field distance for the antenna is calculated based on the Fraunhofer distance and it is found, to be less than 3 mm from the antenna aperture. Therefore, all the measurements are taken in the far field, and hence, there is no near field effect considered here. Two holders are used to fix and elevate each antenna to avoid coupling between the antenna and metal surface of the ME.

To investigate the channel behavior within the empty metal cabinet, we have considered the following four scenarios. *Scenario 1* is an LOS scenario where we use a ME of dimension

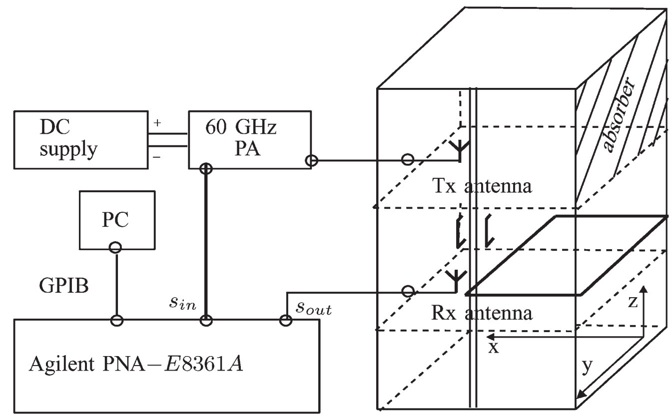

Fig. 2. Measurement setup for channel sounding inside the metal cabinet. The solid parallelogram just above the first level shows the metal plate that has been used in the NLOS scenario. The top right wall is covered with absorber for *scenario 4* (small size cabinet).

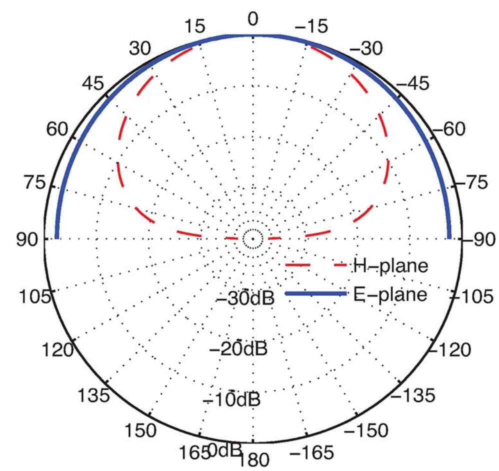

Fig. 3. Field radiated by the TE_{10} mode in open waveguide antenna with respect to θ angle.

$100 \times 45 \times 45$ cm^3. *Scenario 2* is an LOS scenario with a ME of a larger dimension, i.e., $100 \times 45 \times 180$ cm^3. *Scenario 3* is a NLOS scenario with the dimensions $100 \times 45 \times 180$ cm^3. *Scenario 4* is an LOS scenario as in *Scenario 1* except that one of the side walls is covered with an absorber (see the illustration in Fig. 2). Absorbers are an alternative physical solution to reduce the channel length which will simplify the required channel equalization. Note that the volume of the ME in *scenario 2* and *scenario 3* is four times larger than the volume of the ME used for *scenario 1* and *scenario 4*. To block the LOS path, and create the NLOS scenario, a 50×45 cm metal separation plate is used in *scenario 3* as illustrated in Fig. 2.

The transmit and receive antennas were placed on a styrofoam (polystyrene) sheet, which acts as vacuum for radio waves and has a negligible effect on the channel behavior. The transmit and receive antennas were supported using clamps (stand holders) with sufficient clearance from the metal surface. The co-axial cables were drawn into the metal cabinet by means of small holes which are just sufficiently large to pass the cable.

For all scenarios, the location of the transmit antenna was kept fixed. The channel was measured at various locations in

TABLE I
RECEIVE ANTENNA CO-ORDINATES

	x-axis	y-axis	z-axis
Scenario 1	15-85 cm; 8 steps	5-30 cm; 6 steps	150,165 cm; 2 steps
Scenario 2	15-85 cm; 8 steps	5-30 cm; 6 steps	40,145 cm; 2 steps
Scenario 3	15-40 cm; 6 steps	5-30 cm; 6 steps	40,145 cm; 2 steps
Scenario 4	15-35 cm; 5 steps	5-30 cm; 6 steps	150,165 cm; 2 steps

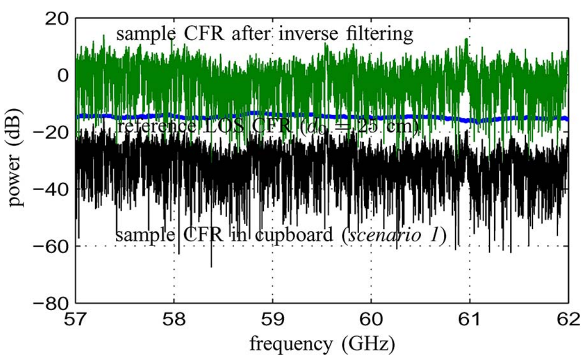

Fig. 4. Sample CFR from *scenario 1* before (lower CFR) and after inverse filtering (upper CFR) and reference CFR with $d_0 = 25$ cm (line in the middle).

3 dimensions, i.e., x, y, z-axes, as specified in Table I. This produced 96, 96, 72, and 60 receiver locations for scenario 1, 2, 3, and 4, respectively. Two elevation steps were used in z-axis, 6 steps in y-axis and 8, 6, and 5 steps in x-axis for different scenarios as shown in Table I.

In *scenario 1* and *scenario 4* the transmit antenna was fixed at co-ordinate $(x_t, y_t, z_t) = (65, 15, 135)$ cm, and in *scenario 2* and *scenario 3* the transmit antenna was located at $(x_t, y_t, z_t) = (15, 15, 130)$ cm. The position of the metal plate was at $z \approx 60$ cm and $z \approx 140$ cm for the first and second steps in z-axis in *scenario 3*. In *scenario 4*, the bulky absorbers were limiting the space so less measurements were taken in this scenario and only the RDS spread property has been extracted. The minimum and maximum distances between Tx and Rx are in the range of 1.5 m to 15 cm.

B. Data Processing

Post-processing of the data is required to extract the CIR from the measured FD signals. In principle, this involves an inverse discrete Fourier transform (IDFT). The IDFT includes a window; the resulting impulse response is thresholded to remove paths with small amplitudes. Prior to the IDFT, we cancel the antenna and instrument responses by using an inverse filtering technique [35], [36] which is briefly explained in Appendix A.

Fig. 4 shows the original FD response (CFR) of a sample measurement from *scenario 1*, the FD response after inverse filtering and the FD signal of the truncated reference measurement. The effect of inverse filtering can be observed after calibration plot where the sample CFR is normalized by $R_{fl}(f)$. The change in the power levels after inverse filtering is due to the compensation of antenna and instrument responses.

For model parameters that do not depend on the absolute power (i.e. the small-scale channel model considered in Section IV), we have normalized the received signal to have a maximum value at 0 dB. The dynamic range of the received signal is in the order of 70 dB, where we assume that the noise level is at -70 dB after normalization.

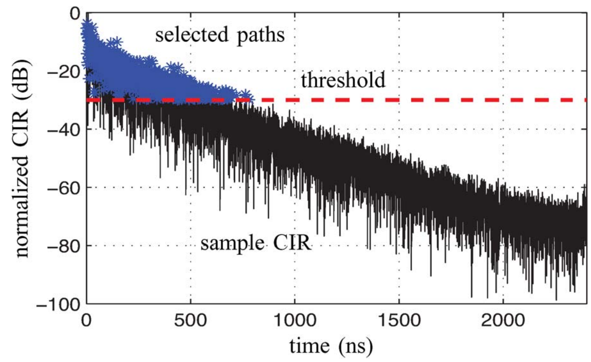

Fig. 5. Sample CIR with 30 dB threshold and received paths for *scenario 1*.

For estimating statistics of the individual link parameters, it is useful to truncate the duration of the channel. We compute the threshold taking into account the noise level, amount of total received power and relevant MPCs [37], [38]. By setting a threshold at 30 dB below the strongest path, more than 98% of the total power is captured. This threshold is still well above the noise level. As an illustration, Fig. 5 shows a normalized received CIR with a threshold at -30 dB. The duration of this channel is still about 800 ns.

III. PATH LOSS MODEL

The large-scale channel model, specifically the path loss model, is essential for any wireless system design to calculate its link budget. For a conventional channel (outdoor or indoor), the path loss model suggests that the average received power decreases exponentially with increasing distance between the transmitter and receiver. This is generally expressed in logarithmic scale as

$$P_L(d)_{dB} = P_L(d_0)_{dB} + 10\alpha \log_{10}\left(\frac{d}{d_0}\right) + X_\sigma. \qquad (2)$$

where $P_L(d)_{dB}$ is the signal power loss at a distance d (m) relative to an arbitrary reference distance d_0 (m), α represents the path loss exponent, and X_σ is a zero-mean Gaussian random variable with standard deviation σ reflecting the attenuation (in dB) caused by shadowing [29], [30]. In fact, the first two terms in (2) together represent the expected path loss and the last term represents the standard deviation. First, we extract a statistical model for the average received power and the path loss exponent and later the shadowing model is derived based on the measurements.

Using the measurements of the received power for different distances between the transmit and receive antennas, we can estimate the path loss exponent α. Accordingly, for each measurement the distance related path loss term $(P_t - P_r)$ is calculated, based on the known transmit power (-68 dB), as shown in Fig. 6(a) which shows that the path loss exponent α is very small (around 0.02–0.002). The reference distance is taken as

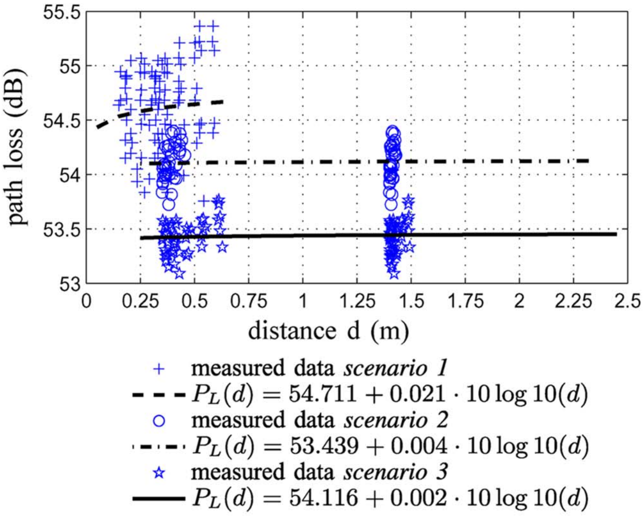

(a)

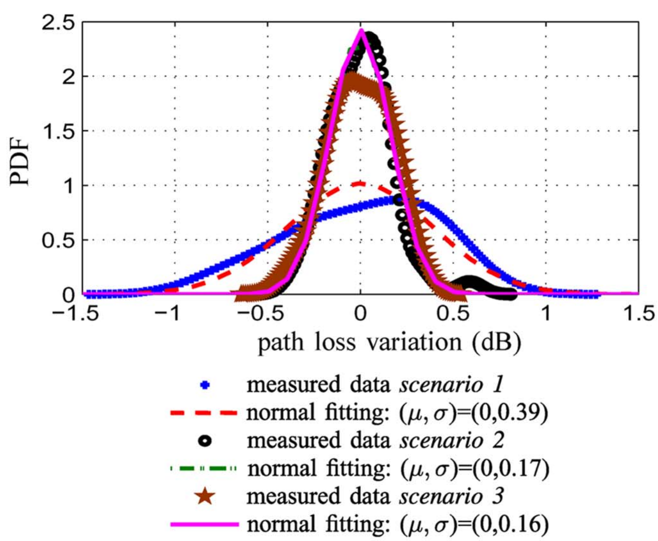

(b)

Fig. 6. Path-loss as function of distance. (a) Path-loss as function of distance. (b) PDF of the path loss variation X_σ.

1 m similar to common indoor environments. This suggests that in such a closed metal environment there is nearly no loss in the received power as function of distance. The same phenomenon is reported in [4] for the environment inside a computer case. Other measurements for NLOS wireless personal area network (WPAN) reported α in the range of 0.04–0.09 [37], [39], while, α in the range 1.6–6 is common for typical indoor systems [29]. According to the Friis formula, the path loss for conventional indoor environments should be larger for transmissions at 60 GHz compared to lower carrier frequencies. However, this is not the case for highly reflective environments such as MEs.

An ideal metal enclosed environment acts as a semi-conservative physical system where the only sources of absorptions are the antennas, cables and stand holders. The waves keep bouncing back and forth, and when the distance between the antennas is increased the received power does not fluctuate because most of the energy reaches the receive antenna either directly or as multipath reflection in the metal cabinet.

Fig. 6(b) shows the probability density function (PDF) of X_σ, i.e., the fluctuation of the path loss around the regression line in Fig. 6(a). It is seen that the PDF approximately follows a normal distribution, with a standard deviation of 0.16–0.39 dB. Among the considered scenarios, the NLOS case (*scenario 3*) shows the smallest variation, and this is due to the larger distances (volume) and the obstructed LOS path. In general there is no noticeable shadowing effect in the environment even in NLOS case, since the reflected paths are almost as strong as LOS path in the ME.

Accordingly, the large scale properties of the channel have been fitted to the well-known log-normal model in (2), and can be used for the wireless system design within empty (not-dense) MEs.

IV. RMS Delay Spread (RDS)

Besides path-loss, the channel can be further characterized by its small-scale properties caused by reflections in the environment, which are modeled as MPCs [29], [30]. We do not consider fading on individual delay paths since the measurements show that there are few MPCs in each resolvable time bin (over the measurement grids), and hence, they are not considered directly in our model. Instead, we consider the statistics of the model parameters for the (normalized) power delay profiles (PDPs) obtained over all the spatial grids i.e., $\mathrm{PDP}^{(g)}(\tau) = |\mathbf{h}^{(g)}(\tau)|^2$, where g denotes the grid (position) point [10]. For example, $g = 1, 2, \cdots, G = 96$, for *scenario 1* and *scenario 2*. The nth multipath component denoted by nth entry of $\mathbf{h}^{(g)}(\tau)$, and it is described by its power a_n^2 and arrival time t_n.

Multipath leads to small-scale fading (variations over short distances due to constructive and destructive additions). The most important model parameters that describe a multipath channel variations are the RMS delay spread and fading properties that can be modeled as the time decay constant and the multipath arrival times in the SV model. We next study these aspects.

Delay spread describes the time dispersion effect of the channel, i.e., the distribution of the received power in time. A large delay spread causes severe inter-symbol interference (ISI) and can deteriorate the system performance. The RDS is a commonly used parameter to characterize this effect [30]. The RDS is obtained by first estimating the individual path parameters $\{(a_n^2, t_n)\}$ for each observation, and then computing

$$t_{rms} = \sqrt{\bar{t^2} - (\bar{t})^2}, \quad \bar{t^\varrho} = \frac{\sum_{n=1}^{N} a_n^2 t_n^\varrho}{\sum_{n=1}^{N} a_n^2},$$

where $\bar{t}$, $\bar{t^2}$, and $\bar{t^\varrho}$ are the first, second and ϱ moment of the delay spread, respectively.

Fig. 7(a) shows the number of received paths for different power thresholds. As expected, the number of received paths (N) increases with increasing threshold level. The received paths are saturated more quickly in *scenario 4* due to the absorbers. In the same way, the RDS increases as the number of collected paths increases (Fig. 7(b)). At a threshold of 30 dB,

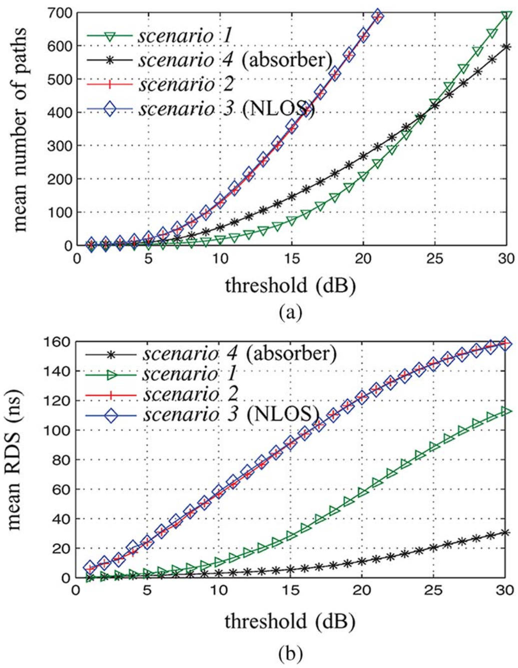

Fig. 7. Number of received paths and RDS for different thresholds. (a) Number of received paths; (b) mean RDS.

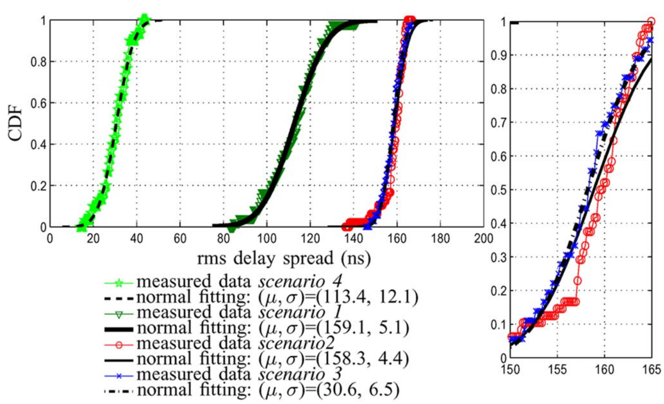

Fig. 8. Cumulative distribution function for RDS of measured channels.

the curves saturate and we used the corresponding value as the estimated RDS. Fig. 8 shows the cumulative distribution function (CDF) of the estimated RDS values for all the four scenarios. The figure also shows the fit to a normal distribution. The mean values of the normal distribution, obtained after fitting, reveals the average length of the channel, and they are 113.4 ns (*scenario 1*), 159.1 ns (*scenario 2*), 158.3 ns (*scenario 3*), and 30.6 ns (*scenario 4*). These mean RDS values for empty metal enclosures are significantly larger than the conventional indoor channels, which are typically between 4–21 ns.

These large values will impact the system design and signal processing within such environments, e.g., the channel equalization and residual inter block interference (IBI) after equalization, and hence, the achievable data rates.

Note that the estimated mean RDS is almost the same for *scenario 2* and *scenario 3*, which shows that there is a clear relation between the volume of such MEs and RDS, independent of LOS and NLOS cases. Also, in *scenario 4* the RDS is reduced by more than 3.5 times as compared to the empty cupboard in *Scenario 1*. These are very interesting results and indicates that even covering one wall with the absorber can reduce the channel length and fading almost to that of a typical indoor environment.

V. Saleh-Valenzuela (SV) Model Parameters

Most current IEEE standard channel models [16], [40] and MIMO channel characterizations [21] for millimeter-wave are based on the extended SV model [28], [41]. In this model, the multipaths are considered as a number of rays arriving within different clusters, and separate power decay constants are defined for the rays and the clusters. This is a very well-known and well-validated model for wireless channels with multipath which was proposed to cover the shortcoming from the traditional Rayleigh (Nakagami) models to describe the statistical PDP. For instance in UWB channel when only the superposition of few MPCs falls within each resolvable delay, the central limit theorem does not hold anymore. This also is the case in our measurements as the high resolution in time makes it less probable to find many MPC within each time bin (channel tap) to derive the fading parameters [10] over each path. Accordingly, we use SV model by extracting the corresponding statistical parameters from the measurement data.

Furthermore, these parameters can be used to generate channel instances with identical statistical properties by defining the average PDP based on the extracted parameters together with the Doppler frequency information. We only derive the SV model parameters for the empty cupboard in *scenarios 1-3* and not for *scenario 4* as the focus of the work is on the empty metal enclosure.

A. Time Decay Constant

A cluster is defined as a group of arrival paths that are reflected from the objects with the same angular profile. One of the common and basic methods to identify the clusters in the channel impulse response (CIR) is by visual observation. We carefully observed the CIRs that were obtained at different positions. Our observation do not show that the MPCs come from multiple clusters, i.e., the power in CIRs is exponentially decaying over the channel length time. This has been observed visually over the measured CIR and verified by the estimated decay parameters. A physical justification comes from the fact that multipath reflections are coming from the (same) walls. Note that if paths from different clusters arrive with the same delay, then the observation technique cannot resolve this ambiguity.

In this case, the average PDP is defined by only one decay parameter γ rather than the common SV model with two decay parameters. Therefore, the proposed model can be given as:

$$\bar{a}_n^2 = \bar{a}_0^2 \exp\left(-t_n/\gamma\right), \quad (3)$$

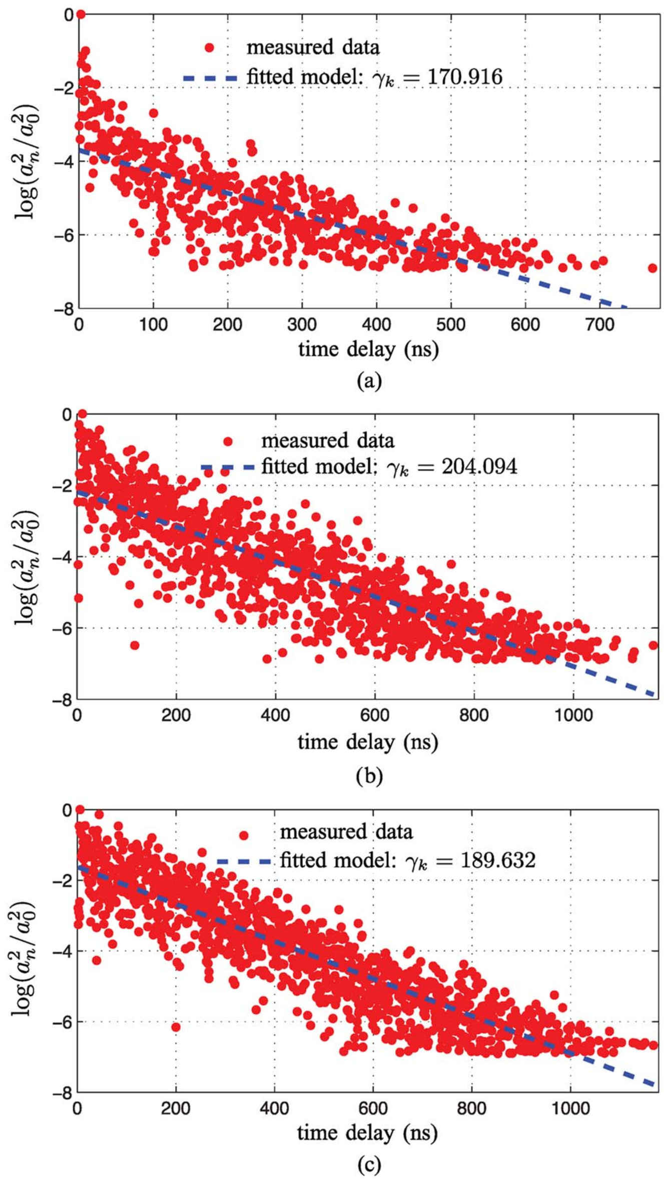

Fig. 9. LS fit for time decay constant γ_k for each measurement. (a) sample measurement in *Scenario 1*; (b) sample measurement in *Scenario 2*; (c) sample measurement in *Scenario 3*.

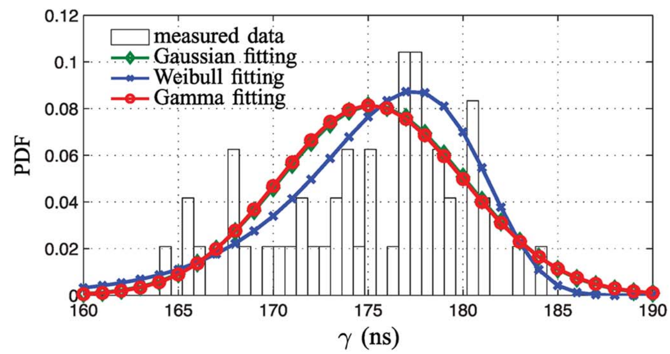

(a) *Scenario 1*
Gaussian$(\mu, \sigma) = (175.2, 4.901)$
Gamma$(\delta, \beta) = (1281, 0.137)$
Weibull $(\zeta, k) = (177.5, 42.28)$

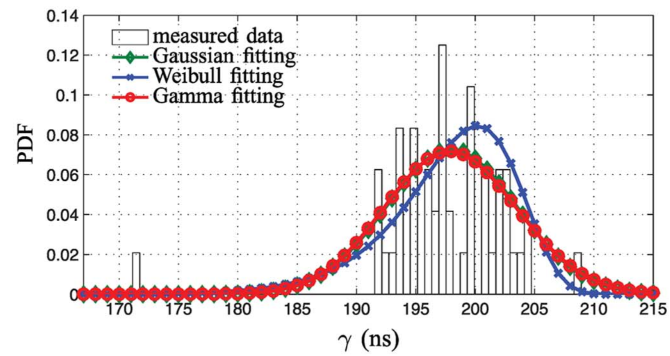

(b) *Scenario 2*
Gaussian$(\mu, \sigma) = (197.9, 5.481)$
Gamma$(\delta, \beta) = (1265, 0.156)$
Weibull$(\zeta, k) = (200.3, 46.05)$

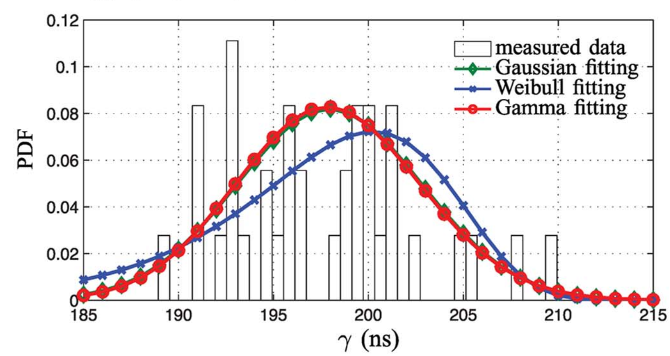

(c) *Scenario 3*
Gaussian$(\mu, \sigma) = (197.9, 4.865)$
Gamma$(\delta, \beta) = (1689, 0.117)$
Weibull $(\zeta, k) = (200.4, 39.37)$

Fig. 10. PDF fittings for time decay constant γ.

where $\bar{a}_0^2$ and $\bar{a}_n^2$ are the (statistical) average power of the first and nth multipath component, respectively, over all different positions and γ is the power decay time constant for arriving rays, assumed as a random variable. To find the decay parameters first we compute the normalized logarithmic PDPs for each measurement. We estimate γ_k for each of the measurement (each position) in every scenario using a least-squares curve fitting on $\log(a_n^2)/\log(a_0^2)$, as shown by the examples in Fig. 9. Time delay instances on the x-axis indicate the arrival time for MPC with respect to the first path.

Based on these estimates for the γ_ks, the PDF for γ is plotted and fitted to Gaussian, Gamma, and Weibull distributions for each considered scenarios, as shown in Fig. 10. These distributions are commonly used to statistically model γ [37], [39].

The best fitted model is chosen as the argument which minimizes the Akaike Information Criterion (AIC) i.e., the distribution that maximizes the log likelihood function in the estimation problem. Accordingly, Gamma has been chosen as the best fit for the γ distribution in *scenario 1* and *scenario 2* while the Weibull distribution is the best candidate in *scenario 3* in a sense that we lose less information by using these models rather than real data.

We use the statistically estimated γ for in rest of the paper. The Gamma distribution is given by

$$f(x|\delta, \beta) = \frac{x^{\delta-1}}{\beta^{\delta}\mathcal{E}(\delta)} \exp\left(-\frac{x}{\beta}\right), \tag{4}$$

where $\mathcal{E}(\delta)$ is a Gamma function, and the parameters δ and β are computed for all scenarios from the empirical data. The Weibull distribution is expressed as

$$f(x|\zeta,k) = \begin{cases} \frac{k}{\zeta^k}\, x^{k-1}\, \exp\big(-(\frac{x}{\lambda})^k\big) & \text{if } x \geqslant 0 \\ 0 & \text{if } x < 0 \end{cases} \tag{5}$$

where the scale and shape parameters are ζ and k, respectively.

There are more accurate techniques to estimate the cluster decay which is specially developed for mm-wave channels when the dynamic range of the system is limited due to the high path-loss and probable wide range of the system that are not applicable for our measurements [42].

B. Multipath Arrival Times

We still need the information on the MPCs arrival time to be able to offer a complete channel model. This gives insight about how dense or sparse the channel is in terms of MPCs and is calculated based on the time difference between two consecutive MPCs. The inter arrival time gives the time between the events of multipath arrivals. The multipath arrival times t_n would be typically modeled as a single Poisson process within each cluster. Having one extended cluster as we observe in our measurements cannot be suitably expressed with single Poisson process. This is due to the fact that the Poisson parameters are considered unrelated to the delays and are treated independently, which does not reflect the reality, so we use different Poisson models for different delay areas.

For a single Poisson process, the inter-arrival times $t_n - t_{n-1}$ are modeled by an exponential PDF as

$$p(t_n|t_{n-1}) = \lambda \exp\big(-\lambda(t_n - t_{n-1})\big) \tag{6}$$

where λ is the mean arrival rate of the MPCs. It is motivated in [37], [43] that when the measured arrival times deviate too much from the single Poisson model, a mixture of two Poisson processes is more suitable for modeling their arrival times. The mixture of two Poisson processes can be expressed as

$$\begin{aligned} p(t_n|t_{n-1}) &= b\,\lambda_1 \exp\big(-\lambda_1(t_n - t_{n-1})\big) \\ &\quad + (1-b)\,\lambda_2 \exp\big(-\lambda_2(t_n - t_{n-1})\big) \end{aligned} \tag{7}$$

where λ_1 and λ_2 are the arrival rates and parameter $0 \le b \le 1$ is the mixing probability.

Fig. 11 shows the corresponding estimated parameters. The inter arrival times are indicated on the x-axis while the logarithmic complementary CDF is shown on the y-axis as it is more informative due to the exponential nature of the Poisson process. As seen, the mixed Poisson process provides a much closer fit to the measured data than the conventional single Poisson process. In fact, parameters b, λ_1 and λ_2, that are estimated and stated in Fig. 11, are used further to generate random arrival time values to be used in the production of the channel instances via simulations.

Similar results are reported in IEEE 802.15.4 [43] for device to device communication for ranges less than 10 m (WPAN).

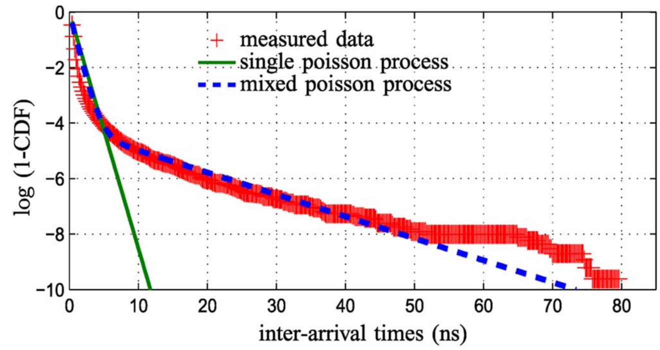

(a) *Scenario 1*: $\lambda = 0.985$, $(\lambda_1, \lambda_2, b) = (0.083, 1.180, 0.015)$.

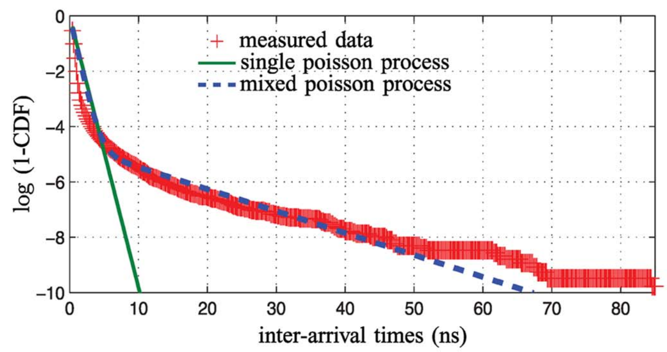

(b) *Scenario 2*: $\lambda = 1.037$, $(\lambda_1, \lambda_2, b) = (0.059, 1.219, 0.008)$.

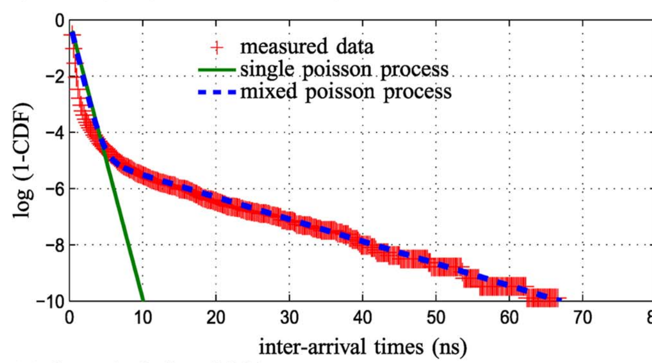

(c) *Scenario 3*: $\lambda = 1.094$, $(\lambda_1, \lambda_2, b) = (0.084, 1.235, 0.009)$.

Fig. 11. Logarithm of the complementary CDF of the inter-arrival times.

Apparently, if the RDS or channel length is large, the arriving paths appear over a wide range of time differences which makes it difficult to be represented by only one Poisson parameter. The results indicate that the inter arrival times are smaller, in general, compared to conventional indoor channels reported in [17], [43]. This indicates the richer scattering environments of the examined ME.

VI. Validation and Evaluation

In this section, we validate our proposed statistical model via Matlab simulations and subsequently we study the behavior of the channel with respect to time. The coherence bandwidth of the measured channel is calculated based on the RDS parameters extracted in Section IV. Finally, channel model parameters

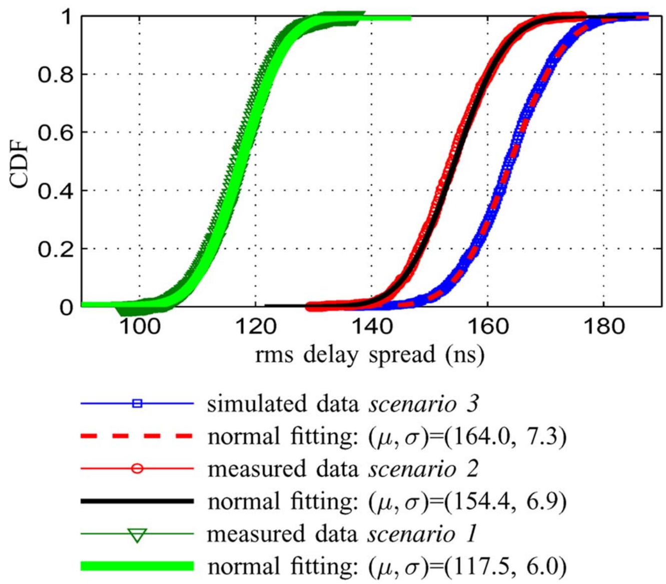

Fig. 12. Cumulative distribution function of RDS based on 1000 simulated channel instances, from left to right are *scenario 1* to *scenario 3* with the fitted model on top of each scenario.

from related measurements are compared with extracted model parameters to give an analogy between different environments and applications.

A. Validation of the Proposed Model via Simulations

We use the estimated SV parameters of the previous section to simulate CIRs and later to compare the properties of these model based simulated channels with the measured channel. This is a straightforward way to validate the proposed statistical channel model. In order to generate a CIR, we need the time instances of multipath arrivals and the energy associated with each path, which are both random variables that are estimated with λ and γ in Section V, respectively. Also, we need to define the number of paths for each channel instance which is a normal random variable itself with certain mean and standard deviation. Having these statistical properties we are able to generate random CIRs. Note that the quality of fit of the PDPs are examined implicitly through the simulation of the RDS parameters as the random PDPs are generated for the simulation of each scenario using the estimated statistical values in Fig. 10. We use the RDS for the validation phase as it comprehensively includes all the parameters of the proposed model.

We have simulated 1000 channels using the proposed model parameters for all three scenarios within the empty ME. The RDS is calculated for these channel instances and the CDF curves with a fitted mean and variance are illustrated in Fig. 12.

In *scenario 1* and *scenario 3* there is a small (almost 5 ns) overestimation (4.5% and 3% error) and in *scenario 2*, an underestimation (3% error) of the mean RDS, in comparison to the measured values which shows an acceptable model estimation error. As a result, the proposed model parameters are valid and can be used to simulate random channels for link design and other studies that require the channel model.

B. Coherence Time and Bandwidth

A good channel model describes the statistical channel strength over both time and frequency domains. The time varying nature of the channel is characterized by the Doppler frequency shift. The resulting coherence time is directly defined by the relative movement (speed) between transmitter and receiver so this is an application specific parameter [30]. The under-test lithography system is part of a mechatronic device in a closed metal environment in which sensors and actuators on a moving platform have to communicate to a controller on the fixed platform. Since movements that occur outside the enclosure do not affect the channel, we expect a slowly time-varying channel with a sufficiently long coherence time. The Doppler shift is defined as $\Delta f_D = \frac{\nu f_c}{c}$, where ν is the relative speed between transmitter and receiver, c is the speed of light, and f_c is the carrier frequency. If we assume a maximum relative speed of 10 ms^{-1}, then the Doppler frequency range is $\Delta f_D = 2$ kHz, and the coherence time of the channel is $\frac{1}{\Delta f_D} = 0.5$ ms.

The coherence BW denoted as B_c gives a sensible insight into the wideband fading model of the system and is directly estimated from the RDS of the channel. A general approximation is $B_c \approx \frac{\iota}{\mu_c}$, where ι depends on the shape of the PDP and μ_c is the so-called mean RDS extracted in Fig. 8. It has been shown in the literature that the channel correlation exceeds 0.9 when $B_c \approx \frac{0.02}{\mu_c}$ [30]. Accordingly, for 90% approximation the mean coherence BW for different scenarios are reported as 176.4, 125.7, 126.3, and 653.6 KHz for scenarios 1 to 4, respectively. Note that the 50% coherence BW is 10 times the aforementioned values.

The coherence BW for the empty metal box is extremely small, this is visually clear from Fig. 4 where the sample CFR shows the dynamic range of almost 30 dB while the reference measurement outside the cupboard is mostly a constant. Note that equalization for such an extreme frequency selective environment is very complex if not impossible. Moreover, despite the general understanding of the 60 GHz propagation environment in outdoor and typical indoor places, the channel does not follow the sparse model in the TD but it can relatively be considered sparse in the FD.

For such a fading channel, orthogonal frequency division multiplexing (OFDM) is an appropriate modulation scheme, and is indeed considered for most of the existing wideband wireless standards including WiMAX, LTE, WiFi, and also for the upcoming new standard for 60 GHz WPAN, i.e., IEEE 802.15.3c. In general, in OFDM the frequency band is divided into several subcarriers such that each subcarrier experiences a flat-fading channel.

Initial simulation results show that OFDM with narrow subbands and frequency domain equalization (FDE) shows an acceptable BER properties in the first three scenarios with respect to typical Rayleigh fading channels. The most distinguishing link budget difference can be pointed out as the long cyclic prefix (time domain guard) that is required for such OFDM system to limit the inter block interference (IBI). In case of the absorber coating, the channel behaves much less dispersive and the performance of the OFDM system is more or less alike in a Rayleigh fading channel of the same length. More details on system design and OFDM performance are considered in future work of authors.

C. Comparison to Other Channel Models

To the best of our knowledge, there are no 60 GHz channel models for very short-range wireless communications (wireless harness) prior to this work. However channel modeling has been done for the IEEE 802.15c standard, for small indoor environment such as cubic offices and kiosks which we discuss here for the sake of comparison. We also compare our obtained results with the channel characterization of a room with metal walls [44] as well as a reflective environment when metallic cabinets are located in the middle of the room [45].

For lower frequencies (3–5 GHz) the results in [11] are interesting for comparison because of the application similarity but the parameters for path loss are expressed in terms of the customized three part model (near, transition and far field) which do not comply with our log-normal model. However, there are some other interesting measurement results for short range wireless applications that we summarize here.

- In [44], path loss and RDS are studied for a 2 GHz band centered at 58 GHz for different room dimensions and properties. In two scenarios, rooms with metal walls are considered with dimensions $44.7 \times 2.4 \times 3.1$ m^3 and $9.9 \times 8.7 \times 3.1$ m^3. For a reference distance of $d_0 = 1$ m, $P_L(d_0)$ around 80 dB and $\alpha < 0.5$ have been reported. Also, the RDS in order of 100 ns is measured which is very close to the results from the metal cabinet.
- In [45], 60 GHz measurements have been conducted in a room with dimensions of $11.2 \times 6.0 \times 3.2$ m^3 with metal reflectors such as metal walls within the room for LOS and NLOS scenarios as well as for different antenna settings. $P_L(d_0)$ with $d_0 = 1$ m, for the Tx-antenna heights of 1.4, 1.9, and 2.4 m are 56.1, 66.8, and 73.1 dB (71.1, 75, and 77.7 dB) for LOS (NLOS), respectively. Path loss exponents of 1.17, 0.18, and 0.61 (5.45, 3.82, and 2.67) are reported for the different Tx elevations for LOS (NLOS) scenarios. As can be seen, small αs in the LOS cases are similar to the ones from the metal cabinet.
- In [46], channel characterization is provided for elevator shafts at 5 GHz with 50 MHz BW, the mean RDS values are reported as 14–60 ns for still elevator, in different locations (buildings) and the maximum RDS is recorded between 144–152 ns when it is moving (different scenarios with Rx inside the elevator car and outside are tested). The RDS values similar to our measurements, are observed here. The derived log distance models show the path loss exponent in the range of 2.75–6.66 when the elevator door is closed and 2.40–5.76 when it is open. Also, the shadowing normal distribution exhibits standard deviation (σ_{P_L}) of 1.89–6.08 dB (door closed) and 2.37–5.52 dB (door open).
- In [5], measurements have been conducted in a computer case at 3.1–10.6 GHz (7.5 GHz BW) for a wireless chip area network (WCAN) application. Parameters α, $P_L(d_0)$ and σ_{P_L} are 1.607, 23.78 dB, and 0.548 dB (2.692, 25.27 dB, and 1.908 dB) for case closed (case open), respectively, for $d_0 = 62$ cm.
- In a similar work in [4], for board-to-board communication in two computer cases (both dense and sparse) the path loss exponent was reported to be negligible where $P_L(d_0)$ and σ_{P_L} appeared as 29.1 dB and 1.4 dB (28.7 dB and 1.4 dB), for the dense (sparse) case, respectively. The 50% coherence BW of the channel and γ are reported as 79 MHz and 3.49 ns (51 MHz and 5.44 ns) for dense (sparse) case. Only one γ parameter is considered in this work similar to a single cluster. The results show a greater coherence BW and consequently smaller time decay constant mostly due to the small volume of the computer case and many absorbing objects inside the metal box. Some losses also can be related to the ventilation holes in the case.

TABLE II
COMPARISON OF VARIOUS CHANNEL PARAMETERS OF THE MEASURED CHANNELS, COMPARED TO IEEE 802.15.3C CHANNEL MODELS. ABBREVIATION "NA" STANDS FOR NOT AVAILABLE AND "-" MEANS NOT APPLICABLE HERE

		Metal cabinet			IEEE 802.15.3c	
		Sc. 1	Sc.2	Sc. 3	CM4	CM9
Parameter	Unit	LOS	LOS	NLOS	NLOS	LOS
$P_L(d_0)$	dB	54.711	53.439	54.116	56.1	NA
α		0.02	0.004	0.002	3.74	NA
σ_{PL}	dB	0.39	0.17	0.16	8.6	NA
$\bar{L}$	ns	113.4	158.3	159.1	NA	NA
Λ	1/ns	-	-	-	0.07	0.044
λ	1/ns	0.985	1.037	1.094	1.88	1.01
Γ	ns	-	-	-	19.44	64.2
γ	ns	175.23	197.99	197.93	0.42	61.1
σ_Γ	ns	-	-	-	1.82	2.66
σ_γ	ns	4.90	5.48	4.86	1.88	4.39

The estimated parameters for our proposed channel model are summarized in Table II, together with the channel model parameters for IEEE 802.15. In this table, the listed parameters are:

$P_L(d_0)$:	path loss at reference distance d_0 (m)
α:	path loss exponent
σ_{P_L}:	path loss log-normal standard deviation
$\bar{L}$:	mean RDS
Λ:	cluster arrival rate
λ:	ray arrival rate (single Poisson fit)
Γ:	power decay constant for clusters
γ:	power decay constant for rays
σ_Γ:	cluster power decay log-normal standard deviation
σ_γ:	ray power decay log-normal standard deviation

The numbers are taken from [40], which provides models for wideband (9 GHz BW) channels at 60 GHz carrier frequency. The reported parameters are selected from the CM4, and CM9 channel models suggested in this document and obtained from measurements in office areas in NLOS scenario, and within a kiosk with LOS, respectively.

It can be seen from Table II that the measured channel in our tested ME differs significantly from the typical wireless channels, as expected. The main distinctions are:

1) Very small path loss exponents in both LOS and NLOS cases,
2) The RDS depends on the ME volume rather than LOS or NLOS,
3) Significantly longer channels or equivalently very large RDS,
4) Arriving rays do not form clusters,
5) Arrival rate is modeled here as a mixed Poisson process.

VII. Summary and Concluding Remarks

In this paper, a comprehensive channel model (large and small scale) is provided for 60 GHz transmission inside a metal enclosure, which is taken as a generic model for the environment inside a lithography system. The FD channel sounding technique with a resolution of 0.2 ns for resolving multipaths and maximum measurable excess delay of 2400 ns is employed to obtain accurate data. A total BW of 5 GHz with a center frequency of 59.5 GHz is used.

The well-known Saleh-Valenzuela model is used to fit the model parameters, which is widely used and validated in the community. Moreover, channel instances are simulated based on the proposed model parameters and the RDS values are shown to comply, in good extent, with the ones from the measured channel. This can serve as a verification of the suggested model.

Distinguishing features of the considered (rather non-conventional) environment are, first of all, the significantly long channels, in the order of 1 μs, together with very rich multipath reflected from the metal walls (small inter arrival times). A statistical model suggests a single cluster nature of the arriving MPCs and the best model fit is proposed as Gamma and Weibull for different scenarios. Further, we observed relatively sparse channel frequency responses with coherence bandwidths of less than 200 kHz, which relates to the high frequency selectivity of the propagation environment. This is a rare phenomenon that has not been observed in other channels before.

The RMS delay spread is shown to be increased by a 40% when the volume of the ME is increased 4 times, accordingly, this leads to 40% decrease in the coherence bandwidth in a larger metal box. The accurate relationship between the enclosure volume/geometry, and the channel parameters yet needs to be verified in future work. Even though, this could be performed by extensive measurements and processing, other analytical approaches such as ray tracing can be employed for further investigation in such a confined environment. Ray tracing may provide more accurate parameters and enables us to study a variety of scenarios without the hassle of sensitive and complex 60 GHz measurements [47], [48]. In our investigation the direction of the antenna does not impact the channel behavior as the open waveguide shows a negligible directivity. Also, the environment of test is somehow symmetrical around a fixed transmitter as the only reflectors are identical metal walls so the expectation is that the power angle profile (PAP) is almost uniform for the measured channels. However, the angular profile of the channel is of a great interest for MIMO applications.

The purpose of this work is to replace cable connections inside a metal enclosed mechatronic system to ease the installation and integration of the machine and also to improve the accuracy and reliability. High data rate and low latency are two critical requirements for lithography devices due to the fast control feedback loop. The latency of the wireless system is determined by the long CIR and the long cyclic prefix in case of OFDM systems. Physical remedies include an absorber coating inside the ME [49], if restrictions on installing such bulky materials inside the mechatronic system are permitted. The measurement results with an absorber coating suggest significant channel shortening.

The proposed statistical channel model helps to understand the challenges related to high data rate wireless communications in such environments. We believe that the outcome of this paper contributes to enrich our understanding of the millimeter-wave propagation properties as well as taking a step towards more user-friendly (plug and play) industrial devices.

Appendix A
Inverse Filtering and Channel Recovery

In this Appendix, we document the selected process of channel estimation from the observed CFRs. Let $x(t)$ be the transmitted signal, which is impaired by the measurement system and the antennas. The received signal $r(t)$ is given by

$$r(t) = x(t) * h_{tx}(t) * h_{sys}(t) * h(t) * h_{rx}(t), \tag{8}$$

where $h_{tx}(t)$ and $h_{rx}(t)$ are the impulse responses of the transmit and receive antennas, $h_{sys}(t)$ is the transfer function of the measurement system and $h(t)$ is the CIR of interest.

The CIR for free space without reflections or obstructions consists of a single LOS path, parameterized by an attenuation and a simple delay equal to the time-of-flight of the signal between the transmit and receive antenna. We can make a recording of the received signal at a known reference distance in free space, and after time gating obtain a reference signal $r_{fl}(t)$, given by

$$r_{fl}(t) \approx x(t) * h_{tx}(t) * h_{sys}(t) * h_{rx}(t)\,, \tag{9}$$

so that

$$r(t) \approx r_{fl}(t) * h(t). \tag{10}$$

More specifically, $r_{fl}(t)$ in (9) absorbs the effect of the antennas and the system (this is not entirely accurate as the directionality of the antennas is ignored). The CIR is obtained from (10) via inverse filtering. Equivalently, in frequency domain, we can obtain the CFR $H(f)$ by

$$H(f) = \frac{R(f)}{R_{fl}(f)}\,. \tag{11}$$

The CIR is then obtained by taking the (windowed) IFFT of $H(f)$ and correction for the delay and attenuation (normalization).

We have obtained a reference LOS signal $r_{fl}(t)$ by placing the transmitter and receiver at a distance of 25 cm outside the metal cabinet (free space). The LOS path was retrieved by time gating the measured signal and truncating it after 50 ns, so as to remove noise and multipaths beyond the direct line of sight.

ACKNOWLEDGMENT

We would like to thank Dr. Marco Spirito and the staff of the Electronics Research Laboratory, TU Delft for providing the channel measurement setup.

REFERENCES

[1] S. Khademi, S. Chepuri, Z. Irahhauten, G. Janssen, and A. van der Veen, "Channel characterization for wideband 60 GHz wireless link within a metal enclosure," in *Proc. IEEE EuCAP*, The Hague, Netherlands, Apr. 2014, pp. 1575–1579.

[2] R. Frank, "Wireless technologies simplify wiring harness," *Auto Electron.*, pp. 17–22, Jul. 2007.

[3] K. Kawasaki *et al.*, "A millimeter-wave intra-connect solution," in *Proc. IEEE ISSCC*, Feb. 2010, pp. 414–415.

[4] J. Karedal, A. Singh, F. Tufvesson, and A. Molisch, "Characterization of a computer board-to-board ultra-wideband channel," *IEEE Commun. Lett.*, vol. 11, no. 6, pp. 468–470, Jun. 2007.

[5] Z. M. Chen and Y.-P. Zhang, "Inter-chip wireless communication channel: Measurement, characterization, and modeling," *IEEE Trans. Antennas Propag.*, vol. 55, no. 3, pp. 978–986, Mar. 2007.

[6] H. Hashemi, "The indoor radio propagation channel," *Proc. IEEE*, vol. 81, no. 7, pp. 943–968, Jul. 1993.

[7] D. Cassioli, M. Win, and A. Molisch, "The ultra-wide bandwidth indoor channel: From statistical model to simulations," *IEEE J. Sel. Areas Commun.*, vol. 20, no. 6, pp. 1247–1257, Aug. 2002.

[8] J. Karedal, S. Wyne, P. Almers, F. Tufvesson, and A. Molisch, "A measurement-based statistical model for industrial ultra-wideband channels," *IEEE Trans. Wireless Commun.*, vol. 6, no. 8, pp. 3028–3037, Aug. 2007.

[9] S. Ghassemzadeh, R. Jana, C. Rice, W. Turin, and V. Tarokh, "Measurement and modeling of an ultra-wide bandwidth indoor channel," *IEEE Trans. Commun.*, vol. 52, no. 10, pp. 1786–1796, Oct. 2004.

[10] A. Molisch, J. Foerster, and M. Pendergrass, "Channel models for ultrawideband personal area networks," *IEEE Wireless Commun.*, vol. 10, no. 6, pp. 14–21, Dec. 2003.

[11] M. Ohira, T. Umaba, S. Kitazawa, H. Ban, and M. Ueba, "Experimental characterization of microwave radio propagation in ICT equipment for wireless harness communications," *IEEE Trans. Antennas Propag.*, vol. 59, no. 12, pp. 4757–4765, Dec. 2011.

[12] N. Nakamoto *et al.*, "Wireless harness inside ICT equipments," in *Proc. 15th ICACT*, Jan. 2013, pp. 135–143.

[13] F. Giannetti, M. Luise, and R. Reggiannini, "Mobile and personal communications in the 60 GHz band: A survey," *Wireless Pers. Commun.*, vol. 10, no. 2, pp. 207–243, Jul. 1999.

[14] R. Daniels and R. Heath, "60 GHz wireless communications: Emerging requirements and design recommendations," *IEEE Veh. Technol. Mag.*, vol. 2, no. 3, pp. 41–50, Sep. 2007.

[15] R. Daniels, J. Murdock, T. Rappaport, and R. Heath, "60 GHz wireless: Up close and personal," *IEEE Microw. Mag.*, vol. 11, no. 7, pp. 44–50, Dec. 2010.

[16] *IEEE Draft Standard for Local and Metropolitan Area Networks - Specific Requirements - Part 11: Wireless LAN Medium Access Control (MAC) and Physical Layer (PHY) Specifications - Amendment 3: Enhancements for Very High Throughput in the 60 GHz Band*, IEEE Std. P802.11ad/D5.0, September 2011, (Draft Amendment based on IEEE P802.11REVmb D10.0) as amended by IEEE 802.11ae D5.0 and IEEE 802.11aa D6.0), Dec. 2011, pp. 1–601.

[17] *IEEE Standard for High Rate Wireless Personal Area Networks (WPANs): Millimeter-Wave-Based Alternative Physical Layer Extension*, IEEE Std. 802.15.3c-2009 (Amendment to IEEE Std 802.15.3-2003), Dec. 2009, pp. c1–187.

[18] P. F. M. Smulders, "Statistical characterization of 60 GHz indoor radio channels," *IEEE Trans. Antennas Propag.*, vol. 57, no. 10, pp. 2820–2829, Oct. 2009.

[19] N. Moraitis and P. Constantinou, "Measurements and characterization of wideband indoor radio channel at 60 GHz," *IEEE Trans. Wireless Commun.*, vol. 5, no. 4, pp. 880–889, Apr. 2006.

[20] M.-S. Choi, G. Grosskopf, and D. Rohde, "Statistical characteristics of 60 GHz wideband indoor propagation channel," in *Proc. PIMRC*, vol. 1, Sep. 2005, pp. 599–603.

[21] C. Gustafson, K. Haneda, S. Wyne, and F. Tufvesson, "On mm-wave multipath clustering and channel modeling," *IEEE Trans. Antennas Propag.*, vol. 62, no. 3, pp. 1445–1455, Mar. 2014.

[22] T. Rappaport *et al.*, "Broadband millimeter-wave propagation measurements and models using adaptive-beam antennas for outdoor urban cellular communications," *IEEE Trans. Antennas Propag.*, vol. 61, no. 4, pp. 1850–1859, Apr. 2013.

[23] W. Fu, J. Hu, and S. Zhang, "Frequency-domain measurement of 60 GHz indoor channels: A measurement setup, literature data, and analysis," *IEEE Instrum. Meas. Mag.*, vol. 16, no. 2, pp. 34–40, Apr. 2013.

[24] S. Geng, J. Kivinen, X. Zhao, and P. Vainikainen, "Millimeter-wave propagation channel characterization for short-range wireless communications," *IEEE Trans. Veh. Technol.*, vol. 58, no. 1, pp. 3–13, Jan. 2009.

[25] M. Peter, W. Keusgen, A. Kortke, and M. Schirrmacher, "Measurement and analysis of the 60 GHz in-vehicular broadband radio channel," in *Proc. VTC*, Oct. 2007, pp. 834–838.

[26] K. O *et al.*, "On-chip antennas in silicon ICs and their application," *IEEE Trans. Electron Devices*, vol. 52, no. 7, pp. 1312–1323, Jul. 2005.

[27] F. Rusek *et al.*, "Scaling up MIMO: Opportunities and challenges with very large arrays," *IEEE Signal Process. Mag.*, vol. 30, no. 1, pp. 40–60, Jan. 2013.

[28] A. A. M. Saleh and R. Valenzuela, "A statistical model for indoor multipath propagation," *IEEE J. Sel. Areas Commun.*, vol. 5, no. 2, pp. 128–137, Feb. 1987.

[29] T. S. Rappaport, *Wireless Communications: Principles and Practice*. Upper Saddle River, NJ, USA: Prentice Hall, 1996.

[30] A. Goldsmith and A. Nin, "Wireless communications," 2005.

[31] MATLAB, version 8.2.0.701 (R2013b). The MathWorks Inc., Natick, MA, USA, 2013.

[32] M. Patzold, A. Szczepanski, and N. Youssef, "Methods for modeling of specified and measured multipath power-delay profiles," *IEEE Trans. Veh. Technol.*, vol. 51, no. 5, pp. 978–988, Sep. 2002.

[33] J. Parsons, D. Demery, and A. Turkmani, "Sounding techniques for wideband mobile radio channels: A review," in *Proc. IPCSV*, vol. 138, no. 5, pp. 437–446, Oct. 1991.

[34] C. A. Balanis, *Antenna Theory: Analysis and Design*. New York, NY, USA: Wiley, 1982.

[35] Z. Irahhauten, *Ultra-Wideband Wireless Channel: Measurements, Analysis and Modeling*. Dept. EEMCS, Delft Univ. Technol., Lund, Sweden, 2008.

[36] A. Siamarou and M. Al-Nuaimi, "A wideband frequency-domain channel-sounding system and delay-spread measurements at the license-free 57 to 64 GHz band," *IEEE Trans. Instrum. Meas.*, vol. 59, no. 3, pp. 519–526, Mar. 2010.

[37] Z. Irahhauten, H. Nikookar, and G. J. M. Janssen, "An overview of ultra wide band indoor channel measurements and modeling," *IEEE Microw. Wireless Compon. Lett.*, vol. 14, no. 8, pp. 386–388, Aug. 2004.

[38] Z. Irahhauten, A. Yarovoy, G. J. M. Janssen, H. Nikookar, and L. Ligthart, "Suppression of noise and narrowband interference in UWB indoor channel measurements," in *Proc. ICU*, 2005, pp. 108–112.

[39] Z. Irahhauten, A. Yarovoy, G. Janssen, H. Nikookar, and L. Ligthart, "Ultra-wideband indoor propagation channel: Measurements, analysis and modeling," in *Proc. EuCAP*, Nov. 2006, pp. 1–6.

[40] "Task group 3c (TG3c) channel modeling sub-committee final report," IEEE P802.15 working group for wireless personal area networks (WPANs), Tech. Rep., Mar. 2007.

[41] Q. Spencer, M. Rice, B. Jeffs, and M. Jensen, "A statistical model for angle of arrival in indoor multipath propagation," in *Proc. IEEE 47th VTC*, 1997, pp. 1415–1419.

[42] C. Gustafson, D. Bolin, and F. Tufvesson, "Modeling the cluster decay in mm-wave channels," in *Proc. 8th EuCAP*, Apr. 2014, pp. 804–808.

[43] *IEEE Standard for Information Technology - Telecommunications and Information Exchange Between Systems - Local and Metropolitan Area Networks Specific Requirements Part 15.4: Wireless Medium Access Control (MAC) and Physical Layer (PHY) Specifications for Low-Rate Wireless Personal Area Networks (LR-WPANS)*, IEEE Std. 802.15.4/2003, 2003, pp. 1–670.

[44] P. Smulders and A. Wagemans, "Wideband indoor radio propagation measurements at 58 GHz," *Electron. Lett.*, vol. 28, no. 13, pp. 1270–1272, Jun. 1992.

[45] H. Yang, M. H. A. J. Herben, and P. F. M. Smulders, "Impact of antenna pattern and reflective environment on 60 GHz indoor radio channel characteristics," *IEEE Antennas Wireless Propag. Lett.*, vol. 4, pp. 300–303, 2005.

[46] R. Sun and D. Matolak, "Characterization of the 5-GHz elevator shaft channel," *IEEE Trans. Wireless Commun.*, vol. 12, no. 10, pp. 5138–5145, Oct. 2013.

[47] J. Liberti and T. Rappaport, "A geometrically based model for line-of-sight multipath radio channels," in *IEEE 46th Veh. Technol. Conf. Mobile Technol. Human Race*, Apr. 1996, vol. 2, pp. 844–848.

[48] C.-F. Yang, B.-C. Wu, and C.-J. Ko, "A ray-tracing method for modeling indoor wave propagation and penetration," *IEEE Trans. Antennas Propag.*, vol. 46, no. 6, pp. 907–919, Jun. 1998.

[49] O. Hashimoto, T. Abe, Y. Hashimoto, T. Tanaka, and K. Ishino, "Realization of resistive-sheet type wave absorber in 60 GHz frequency band," *Electron. Lett.*, vol. 30, no. 8, pp. 657–658, Apr. 1994.

Seyran Khademi (S'11) received the B.S. degree in electrical engineering, with communications minor, from Tabriz University, Iran, in 2005 and the M.Sc. degree from Chalmers University of Technology, Gothenburg, Sweden, in 2010. She is currently working toward her Ph.D. degree with the Circuits and Systems Group, Delft University of Technology, Delft, The Netherlands. Her research interest is in signal processing applications for wireless communications, optimization techniques, MIMO-OFDM systems, beamforming, 60-GHz technology, and audio and speech processing.

Sundeep Prabhakar Chepuri (S'11) was born in India in 1986. He received the B.E. degree (with distinction) from the P.E.S. Institute of Technology, Bangalore, India, in 2007, and the M.Sc. degree (*cum laude*) in electrical engineering from Delft University of Technology, Delft, The Netherlands, in 2011. He is currently working toward the Ph.D. degree with the Circuits and Systems Group, Faculty of Electrical Engineering, Mathematics and Computer Science, Delft University of Technology. During 2007–2009, he was at Robert Bosch India. During 2010–2011, he was with Holst Centre/imec-nl, Eindhoven, The Netherlands. His research interest is in signal processing for communications and networks. He was a recipient of the Student Paper Award at the 2015 International Conference on Acoustics, Speech, and Signal Processing.

Zoubir Irahhauten (M'03) received the M.Sc. and Ph.D. degrees in electrical engineering from Delft University of Technology (TU Delft), Delft, The Netherlands, in 2002 and 2009, respectively. In 2002, he joined the International Research Center for Telecommunications and Radar as a Researcher. In 2007, he joined, as a Postdoctoral Researcher, the Circuits and Systems Group, TU Delft, where he was involved in underwater communication and positioning systems. He is currently with the Mobile Innovation Radio Group, KPN, Den Haag, The Netherlands. His research interests include wireless channel modeling, UWB communications, and antenna design and positioning.

Gerard J.M. Janssen (M'93) received the M.Sc.E.E. degree from Eindhoven University of Technology, Eindhoven, The Netherlands, in 1986 and the Ph.D. degree from Delft University of Technology, Delft, The Netherlands, in 1998. He is currently an Associate Professor with the Circuits and Systems Group, Delft University of Technology. His research interests are in wireless communication, particularly narrow-band multiuser detection, digital modulation techniques, channel modeling, diversity techniques, and ultrawideband communications and positioning.

Alle-Jan van der Veen (F'05) was born in The Netherlands in 1966. He received the Ph.D. degree (*cum laude*) from TU Delft, Delft, The Netherlands, in 1993. Throughout 1994, he was a Postdoctoral Scholar at Stanford University. He is currently a Full Professor of signal processing at TU Delft. His research interests are in array signal processing, with applications to wireless communications and radio astronomy. He was the Chairman of the IEEE Signal Processing Society (SPS) Signal Processing for Communications Technical Committee (2002–2004) and chaired the IEEE SPS Fellow Reference Committee in 2011–2013. He was the Technical Cochair of ICASSP 2011 (Prague). He was also an Editor-in-Chief of the IEEE SIGNAL PROCESSING LETTERS (2002–2005) and the IEEE TRANSACTIONS ON SIGNAL PROCESSING (2006–2008). He was the recipient of a 1994 and a 1997 IEEE SPS Young Author Paper Award.